A unified approach to the modelling of intraparticle diffusion in adsorption processes*

R. Krishna

Department of Chemical Engineering, University of Amsterdam, Nieuwe Achtergracht 166, 1018 WV Amsterdam, The Netherlands

Bulk, Knudsen and surface diffusion of multicomponent mixtures inside porous media are described in a consistent manner using the Maxwell–Stefan formulation. By using several practical examples it is demonstrated that the simple Fick formulation is generally inadequate for the description of intraparticle diffusion because it can fail even at *a qualitative level* to describe the observed phenomena.

Keywords: intraparticle diffusion; multicomponent mixtures; Knudsen diffusion; surface diffusion; Fick's law

Introduction

A proper description of intra-particle diffusion of multicomponent mixtures is essential in the simulation and design of PSA processes[1,2]. In general, we need to describe diffusion inside macro- and micro-pores (see *Figure 1*) and, in practice, we need to distinguish three fundamentally different diffusion mechanisms inside the pores of an adsorbent (*Figure 2*):

1 Bulk, 'free space' or free molecular diffusion that becomes significant for large pore sizes and high system pressures; here molecule–molecule collisions dominate over molecule–wall collisions.
2 Knudsen diffusion that becomes predominant when the mean free path of the molecular species is much larger than the pore diameter and hence molecule–wall collisions become important.
3 Surface diffusion of adsorbed molecular species along the pore wall surface; this mechanism of transport becomes dominant for micro-pores and for strongly adsorbed species.

Bulk and Knudsen diffusion mechanisms occur in series and it is always prudent to take both mechanisms into account rather than assume that one or other mechanism is 'controlling'. Surface diffusion occurs in parallel with the other two mechanisms and its contribution to the total species flux may be quite significant in many cases (as will be seen later). Within the micro-pores the dominant mechanism is surface diffusion. It is for this reason that surface diffusion is also referred to as micropore diffusion in the literature[3]. The pressure gradient inside the particle is not always negligible and this pressure gradient gives rise to viscous, or Darcy flow. *Figure 3* shows the various contributions to the flux of the species inside the particle.

First consider the modelling of bulk and Knudsen diffusion.

Combined bulk and Knudsen diffusion

It is now generally agreed that the correct description of combined bulk and Knudsen diffusion is given by the dusty gas model (see references 4 and 5). The principle behind the dusty gas model is quite simple. The pore wall ('medium') is pictured as consisting of giant molecules ('dust'), uniformly distributed in space. These dust molecules are considered to be a dummy, or pseudo, species $n+1$ in the n-component gaseous mixture. To develop the transport relations we balance the force exerted on any species i in the multicomponent mixture and the friction experienced with the other species during the motion of species i:

$$-\nabla\mu_i = RT\sum_{j=1}^{n} x_j\frac{(\boldsymbol{v}_i-\boldsymbol{v}_j)}{Đ_{ij}} + RTx_{n+1}\frac{(\boldsymbol{v}_i-\boldsymbol{v}_{n+1})}{Đ_{i,n+1}}$$

$$i = 1, 2, \ldots n \qquad (1)$$

Here $-\nabla\mu_i$ is the force exerted per mole of species i. This force is balanced by friction between the species i and j and by the friction between the diffusing species i and the wall (= pseudo-species $n+1$). The vectors $\boldsymbol{v}_i$ and $\boldsymbol{v}_j$ are the velocities of species i and j with respect to the adsorbent particle. The parameters $RT/Đ_{ij}$ and $RT/Đ_{i,n+1}$ can be interpreted as the drag coefficients representing molecule–molecule interactions and

*Paper presented at the symposium 'Gas Separation by PSA', Twente, The Netherlands, 14 February 1992.

0950-4214/93/020091-14

Nomenclature

a_{micro}	Surface area of microporous crystallites per unit volume of particle ($m^2\,m^{-3}$)
b_i	Constant in Langmuir isotherm (Pa^{-1})
$\mathscr{B}$	Permeability of porous medium (m^2)
$[B]$	Matrix of inverted Maxwell–Stefan diffusivities ($m^{-2}\,s$)
$[B^{b+K}]$	Matrix of inverted Maxwell–Stefan diffusivities for combined bulk and Knudsen diffusion ($m^{-2}\,s$)
$[B^s]$	Matrix of inverted Maxwell–Stefan diffusivities for surface diffusion ($m^{-2}\,s$)
c	Molar concentration of the bulk fluid mixture ($mol\,m^{-3}$)
c_i	Molar concentration of species i in bulk fluid ($mol\,m^{-3}$)
c_i^s	Surface concentration of species i ($mol\,m^{-2}$)
c_i^{sat}	Surface concentration of species i at saturation ($mol\,m^{-2}$)
c^{sat}	Total saturation concentration of surface, $c^{sat} = \Sigma_{i=1}^{n} c_i^{sat}$ ($mol\,m^{-2}$)
d_0	Pore diameter (m)
d_p	Particle diameter (m)
D	Fick diffusivity in binary fluid mixture ($m^2\,s^{-1}$)
D_i^s	Fick surface diffusivity of species i($m^2\,s^{-1}$)
$[D]$	Matrix of Fick diffusivities ($m^2\,s^{-1}$)
$[D^{total}]$	Combined matrix of intraparticle Fick diffusivities ($m^2\,s^{-1}$)
$Đ_{12}$	Maxwell–Stefan diffusivity in bulk fluid phase ($m^2\,s^{-1}$)
$Đ_{i,Kn}$	Knudsen diffusivity of component i ($m^2\,s^{-1}$)
$Đ_i^s$	Maxwell–Stefan surface diffusivity of species i ($m^2\,s^{-1}$)
$Đ_{ij}^s$	Maxwell–Stefan counter-sorption diffusivity ($m^2\,s^{-1}$)
$D_{i,eff}^s$	Effective surface diffusivity ($m^2\,s^{-1}$)
D_{ref}	Reference value of intra-particle diffusivity ($m^2\,s^{-1}$)
Fo	Fourier number
$[I]$	Identity matrix
J_0	Bessel function of zero order
K_i	Distribution coefficient for sorption isotherm
m	Index in Equation (71)
M_i	Molar mass of species i ($kg\,mol^{-1}$)
n	Number of diffusing species
$[L]$	Matrix of Onsager coefficients ($m^2\,s^{-1}$)
N_i	Molar flux of species i in a stationary coordinate frame of reference ($mol\,m^{-2}\,s^{-1}$)
N_i^s	Surface flux of adsorbed species i ($mol\,m^{-1}\,s^{-1}$)
p	System pressure (Pa)
p_i	Partial pressure of species i (Pa)
q_i	Adsorbate loading ($mol\,kg^{-1}$)
r_c	Radius of micro-porous crystals (m)
R	Gas constant (8.314 $J\,mol^{-1}\,K^{-1}$)
t	Time (s)
T	Absolute temperature (K)
$\boldsymbol{v}_i$	Velocity of the diffusing species i ($m\,s^{-1}$)
v_1, v_2	z-coordinate velocities of species 1 and 2 ($m\,s^{-1}$)
$\boldsymbol{v}$	Molar average mixture velocity, $\boldsymbol{v} = \Sigma_{i=1}^{n} x_i \boldsymbol{v}_i$ ($m\,s^{-1}$)
x_i	Mole fraction of species i
Δx_i	Composition difference across diffusion distance
∇x_i	Gradient of the component mole fraction
z	Direction coordinate (m)

Greek letters

Γ	Thermodynamic correction factor for binary mixture
$[\Gamma]$	Matrix of thermodynamic factors
δ	Length of diffusion path (m)
δ_{ij}	Kronecker delta (1 if $i = j$; 0 if $i \neq j$)
η	Fluid mixture viscosity (Pa s)
θ_i	Fractional surface occupancy of component i, $\theta_i \equiv c_i^s/c^{sat}$
θ_t	Total surface occupancy of n species, $\theta_t = \Sigma_{j=1}^{n} \theta_j$
θ_i^{sat}	Fractional surface occupancy of component i at saturation, $\theta_i^{sat} \equiv c_i^{sat}/c^{sat}$
λ	Lateral displacement during surface diffusion (m)
μ_i	Chemical potential of i in bulk fluid ($J\,mol^{-1}$)
μ_i^s	Surface chemical potential of species i ($J\,mol^{-1}$)
ν_1	Jump frequency of component 1 (s^{-1})
ξ_m	Roots of the zero order Bessel function $J_0(\xi_m) = 0$
ρ_p	Particle density ($kg\,m^{-3}$)
σ_{ij}	Collision diameter for species $i - j$ (m)

Subscripts

i, j	Components in mixture
eff	Effective parameter
Kn	Knudsen coefficient
t	Total mixture
viscous	Viscous flow parameter
$x_1 \to 0$	For vanishing small concentration of species 1
$x_1 \to 1$	For almost pure component 1
δ	Position $z = \delta$
0	Position $z = 0$
$n + 1$	Pseudo-species

Superscripts

0	Standard state
b + K	Combined bulk and Knudsen diffusion
free space	Parameters in free space
s	Surface
sat	Saturation
total	Combined bulk, Knudsen and surface diffusion parameter

molecule–wall interactions, respectively. The Maxwell–Stefan diffusivities $Đ_{ij}$ and $Đ_{i,n+1}$, defined by Equations (1), are therefore to be interpreted as inverse drag coefficients.

The principal idea behind the derivation of the dusty gas model, i.e. setting up a balance between the force exerted on a species and the friction experienced during the movement of this species in the mixture, originates from the independent works of James Clerk Maxwell[6] and Josef Stefan[7], which is more than a century old. The Maxwell–Stefan diffusivities $Đ_{ij}$ can be related to the

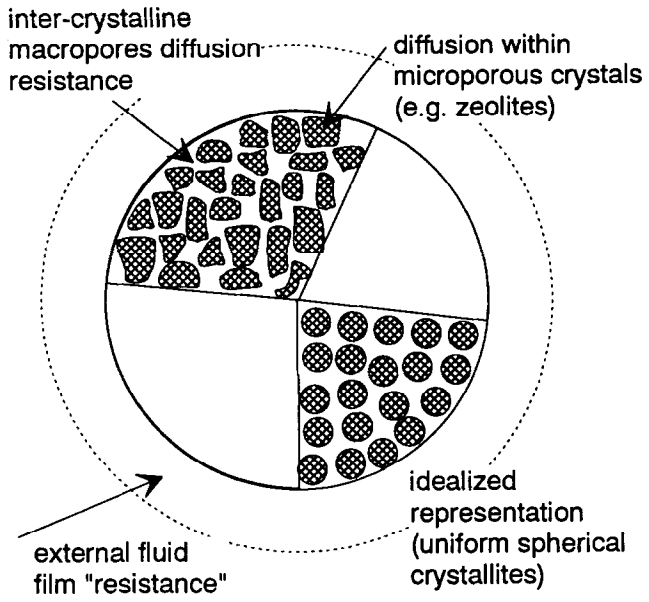

Figure 1 Schematic diagram of adsorbent or catalyst particle depicting the three main diffusion resistances (after Ruthven[3])

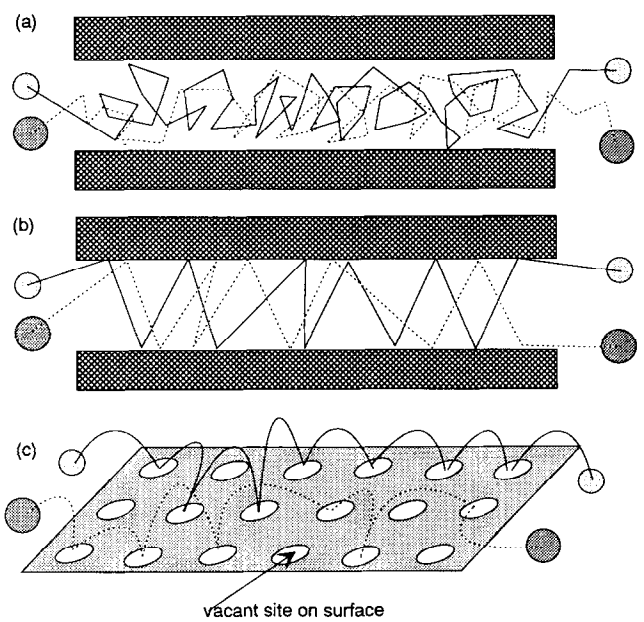

Figure 2 Three distinct mechanisms by which molecular species get transported within an adsorbent or catalyst particle: (a) bulk diffusion; (b) Knudsen diffusion; and (c) surface diffusion of adsorbed species along the surface of the pores

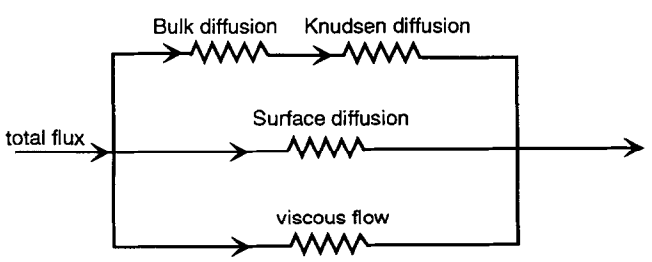

Figure 3 Electric analogue circuit picturing the flux of the diffusing species within a porous medium (after Mason and Malinauskas[5])

molecular diffusivities in 'free' space by

$$Đ_{ij} = \frac{\text{(constriction factor)}}{\text{(tortuosity)}} Đ_{ij}^{\text{free space}} \tag{2}$$

The free space bulk diffusivity values can be estimated from the kinetic gas theory[8], which shows that

$$Đ_{ij}^{\text{free space}} \propto \frac{T^{3/2}(1/M_i + 1/M_j)^{1/2}}{p\sigma^2} \tag{3}$$

It is usual to define the Knudsen diffusivity

$$Đ_{i,\text{Kn}} \equiv \frac{D_{i,n+1}}{x_{n+1}} \tag{4}$$

For a cylindrical pore of diameter d_0, the Knudsen diffusivity can be estimated from the kinetic gas theory. The result is

$$Đ_{i,\text{Kn}} = \frac{d_0}{3}\left(\frac{8RT}{\pi M_i}\right)^{1/2} \quad \text{(for cylindrical pores)} \tag{5}$$

where M_i is the molar mass of species i. In general, for non-cylindrical pores the Knudsen diffusivity has to be estimated from

$$Đ_{i,\text{Kn}} = \frac{\text{(constriction factor)}}{\text{(tortuosity)}} \frac{d_0}{3}\left(\frac{8RT}{\pi M_i}\right)^{1/2} \tag{6}$$

For ideal gas mixtures the chemical potential gradient is

$$\nabla\mu_i = RT\nabla \ln(p_i) \tag{7}$$

We introduce the molar fluxes, defined per square metre of adsorbent cross sectional area,

$$N_i \equiv c_i v_i = \left(\frac{p}{RT}\right) x_i v_i \tag{8}$$

The dust molecules are held stationary in space and therefore

$$v_{n+1} = 0 \tag{9}$$

Equations (1) and (7)–(9) may be combined to give

$$-\frac{1}{RT}\nabla p_i = \sum_{\substack{j=1 \\ j\neq i}}^{n} \frac{x_j N_i - x_i N_j}{Đ_{ij}} + \frac{N_i}{Đ_{i,\text{Kn}}} \quad i = 1, 2, \ldots n \tag{10}$$

Let us cast Equation (10) in n-dimensional matrix form:

$$-\frac{1}{RT}(\nabla p) = [B^{b+K}](N) \tag{11}$$

The elements of the matrix $[B^{b+K}]$ are given by

$$B_{ii}^{b+K} = \frac{1}{Đ_{i,\text{Kn}}} + \sum_{\substack{j=1 \\ j\neq i}}^{n} \frac{x_j}{Đ_{ij}} \quad i = 1, 2, \ldots n$$

$$B_{ik}^{b+K} = -\frac{x_i}{Đ_{ik}} \quad \underset{(i\neq k)}{i,k} = 1, 2, \ldots n \tag{12}$$

The bulk and Knudsen diffusivities, $Đ_{ij}$ and $Đ_{i,\text{Kn}}$, respectively, are influenced differently by the system parameters. Let us examine the two limiting cases of bulk diffusion and Knudsen diffusion.

Bulk diffusion control

The bulk diffusivity $Đ_{ij}$ is inversely proportional to the system pressure (cf. Equation (3)) and therefore with increasing system pressure the molecule–molecule interactions become of increasing importance. At sufficiently high pressure the Knudsen contribution may be neglected and the matrix $[B^{b+K}]$ reduces to:

$$B_{ii}^{b+K} = \sum_{\substack{j=1 \\ j\neq i}}^{n} \frac{x_j}{Đ_{ij}} \quad i = 1, 2, \ldots n$$

$$B_{ik}^{b+K} = -\frac{x_i}{Đ_{ik}} \quad \underset{(i\neq k)}{i,k} = 1, 2, \ldots n \tag{13}$$

The Knudsen diffusivity is proportional to the pore diameter d_0 and for large pore diameter the frictional contribution due to molecule–wall collisions may be neglected. In this case too the matrix $[B^{b+K}]$ reduces to that given by Equations (13).

For systems containing three or more species the diffusion behaviour can be very peculiar and not conform to normal Fickian expectations. This peculiar multicomponent behaviour will be demonstrated by considering a simple and illuminating set of experiments conducted by Duncan and Toor[9]. These authors examined diffusion in an ideal ternary gas mixture hydrogen (1)–nitrogen (2)–carbon-dioxide (3). The experimental set-up consisted of a two-bulb diffusion cell (*Figure 4a*). In an experiment that is highlighted here the two bulbs, 1 and 2, had the initial compositions (expressed in mole fractions) given below:

1: $x_1 = 0.50121 \quad x_2 = 0.49879 \quad x_3 = 0.00000$

2: $x_1 = 0.00000 \quad x_2 = 0.50086 \quad x_3 = 0.49914$

The two bulbs were connected by means of a long capillary of 2.08 mm diameter. At time $t = 0$, the stopcock separating the two composition environments at the centre of the capillary was opened and diffusion of the three species was allowed to take place. From the information given in the paper by Duncan and Toor, it is verifiable that the diffusion mechanism prevalent in the capillary is bulk diffusion. Further, the pressure differences between the two bulbs were negligibly small, implying no occurrence of viscous flow. Since the two bulbs are sealed, there was no net transfer flux out of or into the system, i.e. conditions corresponding to equimolar diffusion prevail:

$$v = 0 \quad N_1 + N_2 + N_3 = 0 \tag{14}$$

The composition–time trajectories for each of the three diffusing species in either bulb have been presented in *Figure 4b*. First examine what happens to hydrogen (1) and carbon dioxide (3). The composition–time trajectories are as should be expected; hydrogen diffuses from bulb 1 to bulb 2 and the two compositions approach each other, albeit slowly. Carbon dioxide diffuses from bulb 2 to bulb 1 in the normal expected fashion. The diffusion behaviour of these two species, hydrogen and carbon dioxide, may be termed Fickian, i.e. down their respective composition gradients. There is nothing remarkable in the diffusion behaviour of hydrogen and carbon dioxide.

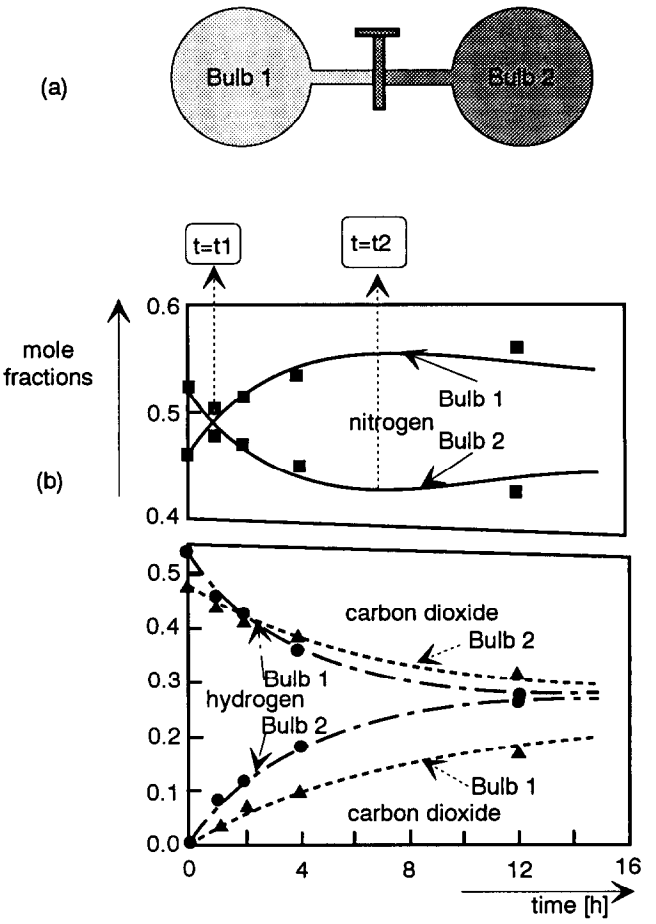

Figure 4 Two-bulk diffusion cell experiment of Duncan and Toor[9]: (a) experimental set-up; (b) composition–time trajectories for the species hydrogen (1)–nitrogen (2)–carbon-dioxide (3)

However, if the composition–time trajectory of nitrogen (2) is examined, several curious phenomena are seen to occur. Initially, at time $t = 0$, the composition of nitrogen in bulb 2 is higher than in bulb 1, so we should expect, following Fickian ideas, that diffusion should take place from bulb 2 to bulb 1, decreasing the composition in bulb 2 and consequently increasing the composition of nitrogen in bulb 1. This expectation is indeed fulfilled during the time interval from $t = 0$ to $t = t1 \approx 1$ h (*Figure 4b*). At the end of this interval, the composition of nitrogen in the two bulbs is identical, and therefore at this point the composition gradient driving force for nitrogen must be zero. At $t = t1$, it was observed experimentally by Duncan and Toor that the diffusion of nitrogen did not cease but, contrary to Fickian expectations, continued further, implying that

$$\nabla x_2 = 0 \quad N_2 \neq 0 \quad t = t1 \tag{15}$$

The bulb 1 composition of nitrogen continued to increase at the expense of bulb 2 composition beyond the point $t = t1$, and this diffusion of nitrogen is in an uphill direction, i.e.

$$\frac{N_2}{-\nabla x_2} > 0 \quad t1 < t < t2 \tag{16}$$

Uphill diffusion of nitrogen continued to take place until $t = t2$, when the composition profiles in either bulb tend to reach a plateau. This plateau implies that the diffusion

flux of nitrogen is zero at this point, despite the fact that there is a large driving force in existence. At $t = t2$:

$$\nabla x_2 \neq 0 \quad N_2 = 0 \quad t = t2 \tag{17}$$

Beyond the point $t = t2$, the diffusion behaviour of nitrogen is 'normal', i.e. the composition of nitrogen in bulb 1 with a higher concentration decreases while the composition of nitrogen in bulb 2 with the lower concentration increases.

Toor[10], in a classic paper, anticipated the three curious phenomena described above and assigned the following names to them:

1 Osmotic diffusion: this is the phenomenon observed at $t = t1$ and described above by Equation (15). Here diffusion of a component takes place despite the absence of a constituent driving force.
2 Reverse diffusion: this phenomenon is observed for nitrogen in the time interval $t1 < t < t2$ and described by Equation (16). Here diffusion of a component takes place in a direction opposite to that dictated by its driving force.
3 Diffusion barrier: this phenomenon is observed at $t = t2$ and is described by Equation (17). Here a component diffusion flux is zero despite the existence of a large driving force.

It should be clear that the use of the Fick formulation, wherein it is assumed that the flux of any species is engendered by its own driving force, i.e.

$$N_i = -\frac{1}{RT} D_i \nabla p_i \quad i = 1, 2, 3 \tag{18}$$

will be totally inadequate to describe the three curious phenomena described above because, in order to rationalize the experimental observations, we must demand the following behaviour of the Fick diffusivity for nitrogen (2):

$D_2 \to \infty$ at the osmotic diffusion point; cf. Equation (15);
$D_2 < 0$ in the region where reverse diffusion occurs, cf. Equation (16);
$D_2 = 0$ at the diffusion barrier, cf. Equation (17).

It must not be forgotten that this strange behaviour of the Fick diffusivity for nitrogen has been observed experimentally for an ideal gas mixture at constant temperature and pressure conditions and for a situation corresponding to equimolar diffusion. In contrast with the Fick formulation, the dusty gas model Equations (10) and (11) are able to model the 'peculiar' behaviour of nitrogen in a straightforward manner, as illustrated below.

First, recognize that for conditions of equimolar diffusion prevalent in the two-bulb diffusion cell experiment, only two of the three fluxes are independent. Eliminating the flux of carbon dioxide (3), N_3, we may re-write Equations (11), neglecting the Knudsen diffusion contribution, as follows:

$$-\frac{1}{RT}\nabla p_1 = (B_{11}^{b+K} - B_{13}^{b+K})N_1 + (B_{12}^{b+K} - B_{13}^{b+K})N_2$$

$$-\frac{1}{RT}\nabla p_2 = (B_{21}^{b+K} - B_{23}^{b+K})N_1 + (B_{22}^{b+K} - B_{23}^{b+K})N_2 \tag{19}$$

where the elements B_{ik}^{b+K} of the matrix $[B^{b+K}]$ are given by Equations (13). For the system hydrogen (1)–nitrogen (2)–carbon-dioxide (3), the Maxwell–Stefan diffusivities of the three binary pairs can be estimated from the kinetic gas theory to be

$$\mathcal{D}_{12} = 8.33 \times 10^{-5}$$

$$\mathcal{D}_{13} = 6.8 \times 10^{-5}$$

$$\mathcal{D}_{23} = 1.68 \times 10^{-5}$$

At the equilibrium composition, the elements of the matrix $[B^{b+K}]$ is estimated to be

$$[B^{b+K}] = \begin{bmatrix} 0.967 & -0.301 & -0.369 \\ -0.6 & 1.786 & -2.975 \\ -0.367 & -1.486 & 3.344 \end{bmatrix} \times 10^4$$

Equations (19) can therefore be written as:

$$-\frac{1}{RT}\nabla p_1 = (1.336N_1 + 0.068N_2) \times 10^4$$

$$-\frac{1}{RT}\nabla p_2 = (2.375N_1 + 4.762N_2) \times 10^4 \tag{20}$$

For constant pressure conditions, $-(RT)^{-1}\nabla p_i$ can be replaced by $-c\nabla x_i$, where c is the total molar concentration of the mixture. Employing matrix inversion, the flux of nitrogen can be written explicitly as $N_2 = -c(-3.83\nabla x_1 + 2.15\nabla x_2) \times 10^5$. This implies that the flux of nitrogen is strongly coupled to the driving force of the component 1. When the driving force of nitrogen $\nabla x_2 = 0$, notice that the flux of nitrogen remains non-zero and equals $N_2 = -cD_{21}\nabla x_1 = -c(3.83 \times \nabla x_1) \times 10^{-5}$. This non-zero flux causes the diffusion of nitrogen beyond the point $t = t1$ (the osmotic diffusion point) in *Figure 4b*. Between $t = t1$ and $t = t2$, $|3.83 \times \nabla x_1| > |2.15 \times \nabla x_2|$ and therefore the direction of nitrogen is against its intrinsic gradient (reverse or uphill diffusion). At the point $t = t2$, $|3.83 \times \nabla x_1| = |2.15 \times \nabla x_2|$ and since these two terms have opposite signs, $N_2 = -c(-3.83 \times \nabla x_1 + 2.15 \times \nabla x_2) \times 10^{-5} = 0$ and nitrogen experiences a diffusion barrier.

What we did above was to transform the Maxwell–Stefan diffusion equations into a matrix generalization of Fick's law to explain the curious effects observed by Duncan and Toor[5]. The path via matrix algebra is not essential. It is possible to explain the behaviour of nitrogen in *Figure 4b* directly by using the force–friction arguments of the Maxwell–Stefan (equivalent to dusty gas) formulation. The driving force of nitrogen is much smaller compared with that of hydrogen and carbon dioxide. The frictional drag exerted by carbon dioxide (3) on nitrogen (2) transport is considerably larger than the frictional drag exerted by hydrogen (1) on nitrogen (2) transport; this can be seen from the fact that $(1/\mathcal{D}_{23}) \gg (1/\mathcal{D}_{12})$. During the time interval $t = t1$ and $t = t2$ the direction in which the driving force of carbon dioxide acts is opposite to that in which the driving force of nitrogen acts. The much larger flux of carbon dioxide drags nitrogen against its intrinsic gradient, uphill. From this reasoning it should be clear that if the components hydrogen and carbon dioxide were switched in the two bulbs, i.e. with driving forces of carbon dioxide and

nitrogen in the same direction, no reverse diffusion of nitrogen would have been observed.

Knudsen diffusion

For low system pressures, intraparticle transport is determined by molecule–wall collisions, or in other words the transport is in the Knudsen regime. The matrix $[B^{b+K}]$ in this case is diagonal:

$$B_{ii}^{b+K} = \frac{1}{\mathcal{D}_{i,Kn}} \quad i = 1, 2, \ldots n$$

$$B_{ik}^{b+K} = 0 \quad \underset{i \neq k}{i,k} = 1, 2, \ldots n \tag{21}$$

For small pore diameters molecule–wall collisions again predominate and in this case too the matrix $[B^{b+K}]$ is given by Equations (21). Combining Equations (1) and (21) we see that for Knudsen-controlled intraparticle diffusion the flux of any species is

$$N_i = -\frac{1}{RT}\mathcal{D}_{i,Kn}\nabla p_i \text{ (Knudsen regime)} \tag{22}$$

i.e. down its own, intrinsic, driving force. The diffusion behaviour may therefore be termed to be Fickian.

The Knudsen diffusion coefficient $D_{i,Kn}$ is independent of pressure (cf. Equation (5)) while the bulk diffusivity is inversely proportional to the pressure (cf. Equation (3)). This implies that with increasing system pressure one moves from the Knudsen diffusion controlled regime to the bulk diffusion controlled regime. On the other hand, it follows from Equation (22) that the component fluxes N_i in the Knudsen regime should be proportional to the total system pressure. From Equations (11) and (13) it follows that the fluxes N_i should be independent of the total system pressure in the limit of bulk diffusion control. The experimental results for diffusion of helium (1) and argon (2) across a porous septum, reported in reference 5 and reproduced in *Figure 5*, confirm the aforementioned expectations. The fluxes of helium and argon can be calculated by solving the dusty gas model Equations (11) and (12). Since the compositions vary along the diffusion path, numerical integration is required in general. However, the correct trends are also obtained by a linearized approach, assuming a constant value for the matrix $[B^{b+K}]$, evaluated at the average composition in the septum. For negligible pressure drop across the septum, the linearized approach for a two-component system leads to the following set of equations:

$$-\left(\frac{p}{RT}\right)\frac{\Delta x_1}{\delta} = B_{11}^{b+K}N_1 + B_{12}^{b+K}N_2$$

$$-\left(\frac{p}{RT}\right)\frac{\Delta x_2}{\delta} = B_{21}^{b+K}N_1 + B_{22}^{b+K}N_2 \tag{23}$$

where $\Delta x_i = x_{i\delta} - x_{i0}$ is the composition difference across the septum of thickness δ. The elements B_{ik}^{b+K} are calculated by using Equations (12). As can be seen in *Figure 5*, the linearized approach provides a reasonable representation of the diffusion behaviour in both Knudsen and bulk diffusion regimes. Better agreement between theory and experiment can be obtained by numerical integration of the dusty gas model equations[5].

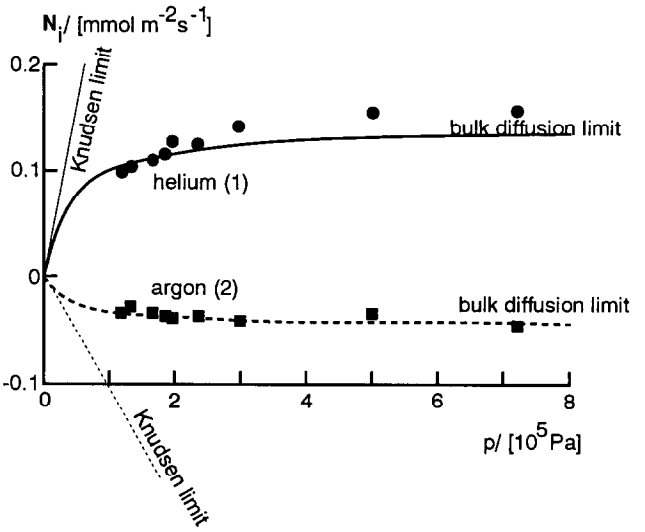

Figure 5 Fluxes of helium (1) and argon (2) across a porous septum as reported in Figure 16 of Mason and Malinauskas[5] as a function of the total system pressure. The experimental conditions were: $\Delta p = 0$; $T = 298.15$ K; $\Delta x_1 = -0.9628$; average composition across septum $\bar{x}_1 = 0.5$; thickness of septum $\delta = 0.00447$ m. The model parameters used in the calculations are: $\mathcal{D}_{1,Kn} = 3.93 \times 10^{-8}$ m^2 s^{-1}; $\mathcal{D}_{2,Kn} = 1.24 \times 10^{-8}$ m^2 s^{-1}; $p\mathcal{D}_{12} = 1.05 \times 10^{-3}$ m^2 s^{-1} Pa. The model calculations for the fluxes of helium and argon were made by using Equations (23), assuming a constant value of the matrix $[B]$ evaluated at the average composition $\bar{x}_1$

In PSA processes it is essential that both bulk and Knudsen diffusion are properly taken into account in the simulations, because the relative importance of these two contributions will change during the cycles.

Viscous flow contribution

Finite pressure gradients within adsorbent particles cause an additional viscous flow contribution to the fluxes. This contribution is

$$N_i^{\text{viscous}} = -\left(\frac{p_i}{RT}\right)\frac{\mathscr{B}}{\eta}\nabla p \tag{24}$$

where $\mathscr{B}$ is the permeability of the medium and η is the mixture viscosity. For a cylindrical pore the permeability is

$$\mathscr{B} = \frac{d_0^2}{32} \tag{25}$$

The viscous flux contribution obtained from Equation (24) has to be added to the fluxes calculated from Equations (10)–(12). Usually, the viscous flow contribution is small and may be neglected. In order to get a feel for the contribution of viscous flow, consider a set of experiments reported in reference 5 for diffusion of the mixture helium (1) and argon (2) across a porous septum. *Figure 6* shows the experimentally determined fluxes of the two components as a function of the pressure difference across the membrane. The total system pressure was maintained constant during the experiments. The linearized theory calculations following Equations (23) and (24) are able to provide a reasonable representation of the experimental results. Neglect of viscous flow leads to a poorer correspondence with experiments.

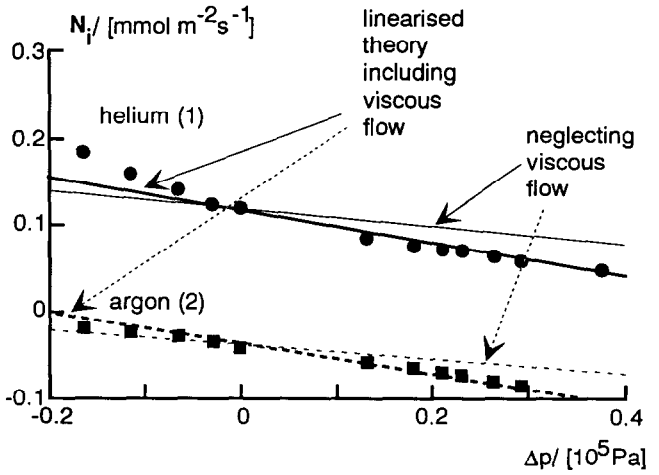

Figure 6 Fluxes of helium (1) and argon (2) across a porous septum as reported in Figure 19 of Mason and Malinauskas[5] as a function of the pressure differential. The experimental conditions were: $\bar{p} = 1.986 \times 10^5$ Pa; $T = 298.15$ K; $\Delta x_1 = -0.9628$; average composition across septum $\bar{x_1} = 0.5$; thickness of septum $\delta = 0.00447$ m. The model parameters used in the calculations are: $\mathcal{D}_{1,Kn} = 3.93 \times 10^{-8}$ m^2 s^{-1}; $\mathcal{D}_{2,Kn} = 1.24 \times 10^{-8}$ m^2 s^{-1}; $p\mathcal{D}_{12} = 1.05 \times 10^{-3}$ m^2 s^{-1} Pa; $\mathscr{B} = 2.13 \times 10^{-18}$ m^2; $\eta = 22.8 \times 10^{-6}$ Pa s. The model calculations for the fluxes of helium and argon were made using Equations (23) and (24), assuming a constant value of the matrix $[B]$ evaluated at the average composition $\bar{x_1}$.

Surface diffusion of adsorbed molecular species

Consider diffusion of n adsorbed molecular species along a surface within the adsorbent pores. In developing a formulation for surface diffusion it is convenient to have a simple physical picture for surface diffusion in mind. Such a simple physical model is depicted in *Figure 2c*, which shows molecules hopping from one adsorption site to another. A description of the hopping model can be found in reference 11. The dusty gas model approach to the description of surface diffusion can be extended by considering the vacant sites to be the $n+1$th pseudo-species in the (surface) system:

$$-\nabla\mu_i^s = RT\sum_{j=1}^{n}\theta_j\frac{(\boldsymbol{v}_i - \boldsymbol{v}_j)}{\mathcal{D}_{ij}^s} + RT\theta_{n+1}\frac{(\boldsymbol{v}_i - \boldsymbol{v}_{n+1})}{\mathcal{D}_{i,n+1}^s} \quad i = 1, 2, \ldots n \tag{26}$$

where $-\nabla\mu_i^s$ is the force acting on species i tending to move it along the surface. The first term on the right of Equation (26) reflects the friction exerted by adsorbate j on the surface motion of adsorbed species i. The second term in Equation (26) reflects the friction experienced by the species i from the vacancies. The θs in Equation (26) represent the fractional occupancies of the adsorbed species. Thus θ_i represents the fractional occupancy of the sites by the adsorbed species i, and θ_{n+1} represent the fraction of unoccupied, vacant, sites

$$\theta_{n+1} = 1 - \theta_1 - \theta_2 - \cdots - \theta_n = 1 - \theta_t \tag{27}$$

In previous analyses[12,13] the author denoted the $\mathcal{D}_{i,n+1}^s$ as the Maxwell–Stefan surface diffusivities. On further reflection, the author feels that it may be preferable to parallel the dusty gas model treatment completely and, by analogy with the definition of the Knudsen diffusivity (cf. Equation 4), the Maxwell–Stefan surface diffusivity ought to be defined as

$$\mathcal{D}_i^s = \frac{\mathcal{D}_{i,n+1}^s}{\theta_{n+1}} \tag{28}$$

Mechanistically, the Maxwell–Stefan surface diffusivity $\mathcal{D}_i^s$ may be related to the displacement of the adsorbed molecular species, λ, and the jump frequency, $\nu_i(\theta_t)$, which in general can be expected to be dependent on the total surface coverage[14–16].

$$\mathcal{D}_i^s = \lambda^2\nu_i(\theta_t) \tag{29}$$

If the jump frequency $\nu_i(\theta_t) = \nu_i(0)$ remains constant, independent of surface coverage, the Maxwell–Stefan surface diffusivity $\mathcal{D}_i^s$ is also independent of surface coverage, i.e.

$$\nu_i(\theta_t) = \nu_i(0) \quad \mathcal{D}_i^s = \lambda^2\nu_i(0) \tag{30}$$

Another possibility is that due to interactions between adsorbed species the jump frequency decreases with surface coverage. If it is assumed that a molecule can migrate from one site to another only when the receiving site is vacant (see Barrer[17]), the chance of this is proportional to $(1 - \theta_t)$, so that

$$\nu_i(\theta_t) = \nu_i(0)(1 - \theta_t) \quad \mathcal{D}_i^s = \lambda^2\nu_i(0)(1 - \theta_t) \tag{31}$$

The coefficients $\mathcal{D}_{ij}^s$ express the adsorbate i–adsorbate j interactions. This coefficient can be considered as representing the facility for counter-exchange, i.e. at an adsorption site the sorbed species j is replaced by the species i. The counter-sorption coefficient D_{ij}^s may therefore be expected to be related to the jump frequency of the species i and j. As a simple (limiting case) model it can be imagined that the counter-sorption diffusivity will be dictated by the lower of the two frequencies ν_i and ν_j, i.e.

$$\mathcal{D}_{ij}^s = \lambda^2/\nu_j(\theta_t) \quad \nu_j < \nu_i \tag{32}$$

Within a single narrow pore of zeolite crystals the mechanism of counter-sorption cannot prevail because there is room for only one type of molecular species at any given time; this is the single-file diffusion mechanism. If, however, the contribution of a bank of parallel pores is taken into account along with cages, the possibility of counter-sorption cannot be ruled out.

Assuming equilibrium between the surface and the bulk fluid we have the following relationship for the surface chemical potential μ_i^s of species i:

$$\mu_i^s = \mu_i = \mu_i^0 + RT\ln(p_i) \tag{33}$$

where μ_i^0 is the chemical potential in the chosen standard state and p_i is the partial pressure of species i in the bulk fluid mixture. The surface chemical potential gradients may be expressed in terms of the gradients of the surface occupancies by introduction of the matrix of thermodynamic factors:

$$\frac{\theta_i}{RT}\nabla\mu_i = \sum_{j=1}^{n}\Gamma_{ij}\nabla\theta_j \quad \Gamma_{ij} \equiv \theta_i\frac{\partial\ln p_i}{\partial\theta_j} \quad i, j = 1, 2, \ldots n \tag{34}$$

For the Langmuir isotherm

$$\theta_i = \frac{c_i^s}{c^{sat}} = \frac{b_i p_i}{1 + \sum_{j=1}^{n} b_j p_j} \quad b_i p_i = \frac{\theta_i}{1 - \theta_t} \tag{35a}$$

the elements of $[\Gamma]$ are:

$$\Gamma_{ij} = \delta_{ij} + \frac{\theta_i}{(1 - \theta_t)} \quad i, j = 1, 2, \ldots n \tag{35b}$$

The surface fluxes N_i^s of the diffusing adsorbed species are defined as:

$$N_i^s = c^{sat} \theta_i v_i \tag{36}$$

where c^{sat} is the total saturation concentration on the surface. The vacant sites can be considered to be stationary, so

$$v_{n+1} = 0 \tag{37}$$

Combining Equations (26)–(37) we obtain, analogous to Equation (10),

$$-\frac{\theta_i}{RT} \nabla \mu_i = \sum_{\substack{j=1 \\ j \neq i}}^{n} \frac{\theta_j N_i^s - \theta_i N_j^s}{c^{sat} \mathcal{D}_{ij}^s} + \frac{N_i^s}{c^{sat} \mathcal{D}_i^s} \quad i = 1, 2, \ldots n \tag{38}$$

which may be cast into n-dimensional matrix notation, analogous to Equation (11), as

$$-c^{sat}[\Gamma](\nabla\theta) = [B^s](N^s) \tag{39}$$

where the (surface) matrix $[B^s]$ has its elements, which are given, analogous to Equations (12), by

$$B_{ii}^s = \frac{1}{\mathcal{D}_i^s} + \sum_{\substack{j=1 \\ j \neq i}}^{n} \frac{\theta_j}{\mathcal{D}_{ij}^s} \quad i = 1, 2, \ldots n$$

$$B_{ik}^s = -\frac{\theta_i}{\mathcal{D}_{ij}^s} \quad i, k = 1, 2, \ldots n \tag{40}$$

If we define a matrix of Fickian surface diffusivities $[D^s]$ by

$$(N^s) = -c^{sat}[D^s](\nabla\theta) \tag{41}$$

we can obtain the following explicit expression for $[D^s]$:

$$[D^s] = [B^s]^{-1}[\Gamma] \tag{42}$$

For a single-file diffusion mechanism, with no possibility of counter-exchange between the adsorbed species i and j, the Equations (38)–(42) simplify to give the following expressions for the Fickian surface diffusivity matrix $[D^s]$

$$[D^s] = \begin{bmatrix} \mathcal{D}_1^s & 0 & 0 & 0 \\ 0 & \mathcal{D}_2^s & 0 & 0 \\ 0 & 0 & \ddots & 0 \\ 0 & 0 & 0 & \mathcal{D}_n^s \end{bmatrix} [\Gamma] \text{ single-file diffusion} \tag{43}$$

A few special cases of Equations (40)–(43) are examined below.

Surface diffusion of a single component

For single-component diffusion, Equations (41)–(42) reduce to the scalar form

$$N_1^s = -c^{sat} \mathcal{D}_1^s \Gamma \nabla\theta_1 \tag{44}$$

where the Fickian surface diffusivity is

$$D_1^s \equiv \frac{N_1^s}{-c^{sat}\nabla\theta_1} = \mathcal{D}_1^s \Gamma \tag{45}$$

For the Langmuir adsorption isotherm the thermodynamic factor Γ is

$$\Gamma = \frac{1}{1 - \theta_1} \tag{46}$$

Combining Equations (45) and (46), we obtain the following expression for the Fickian surface diffusivity

$$D_1^s = \frac{\mathcal{D}_1^s}{(1 - \theta_1)} \tag{47}$$

If the Maxwell–Stefan surface diffusivity $\mathcal{D}_i^s$ decreases with surface coverage following Equation (31), then the Fick surface diffusivity must be independent of surface coverage. On the other hand, if the Maxwell–Stefan surface diffusivity $\mathcal{D}_i^s$ is independent of surface coverage (cf. Equation (30)), the Fickian surface diffusivity should exhibit a sharp increase with θ_1. Such behaviour has been observed by several workers[18], for example for the diffusion of oxygen in carbon molecular sieve[19] (*Figure 7*). In this case it should be clear that adsorption and desorption kinetics should be different from each other. This has been confirmed in practice[20] (*Figure 8*).

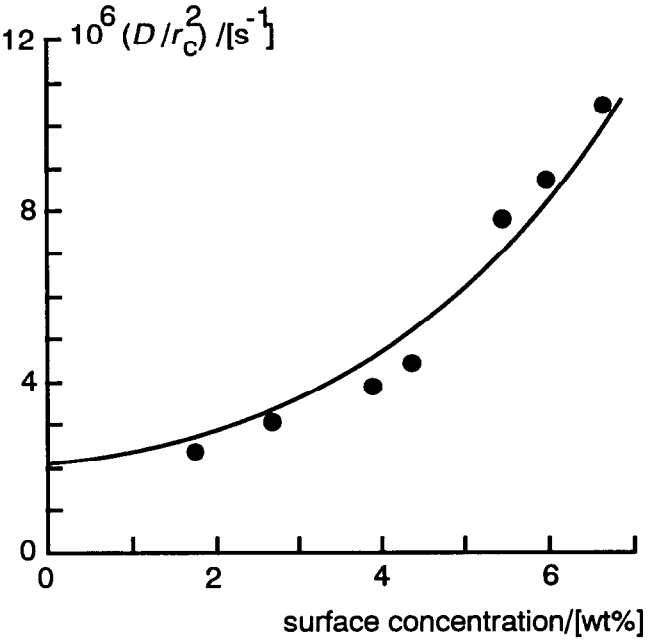

Figure 7 Variation of diffusional time constant with surface concentration for oxygen in Bergbau carbon molecular sieve at 193 K. The theoretical line is from Equation (40), with the thermodynamic factor Γ calculated from the equilibrium isotherm and taking $(\mathcal{D}_1^s/r_c^2) = 2 \times 10^{-6}\,s^{-1}$ where r_c is the crystal radius (after Ruthven[19])

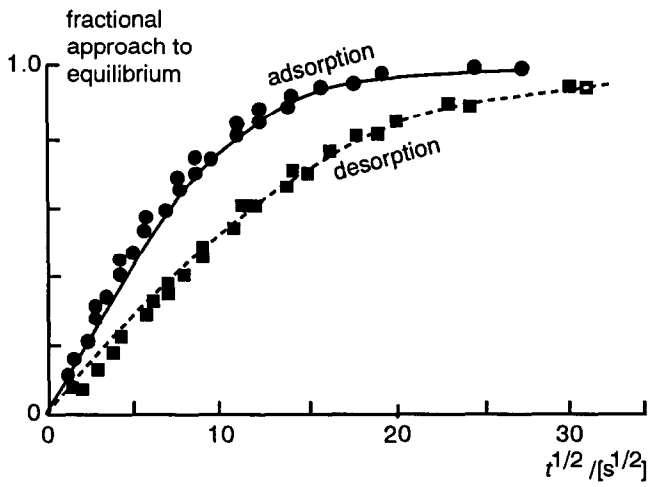

Figure 8 Comparison of experimental and theoretical sorption curves for ethane in 4A zeolite at high concentrations. Theoretical curves for adsorption and desorption drawn taking $(Đ_1^s/r_c^2) = 2.45 \times 10^{-4}\ s^{-1}$. The thermodynamic factor was calculated using Langmuir isotherm (after Garg and Ruthven[20])

Single-file surface diffusion of binary and ternary mixtures

For single-file diffusion involving two components, Equations (41)–(43) reduce to the two-dimensional form

$$(N^s) = -c^{sat}\begin{bmatrix} Đ_1^s & 0 \\ 0 & Đ_2^s \end{bmatrix}[\Gamma](\nabla\theta) \tag{48}$$

If the Langmuir isotherm is used to calculate $[\Gamma]$, we obtain

$$(N^s) = -c^{sat}[D^s](\nabla\theta)\ \ [D^s] = \begin{bmatrix} Đ_1^s & 0 \\ 0 & Đ_2^s \end{bmatrix}\frac{\begin{bmatrix} 1-\theta_2 & \theta_1 \\ \theta_2 & 1-\theta_1 \end{bmatrix}}{1-\theta_1-\theta_2} \tag{49}$$

If we assume that the Maxwell–Stefan surface diffusivities $Đ_i^s$ follow relation (31), the following expression for the 2×2 Fickian surface diffusivity matrix is obtained:

$$[D^s] = \lambda^2\begin{bmatrix} v_1(0) & 0 \\ 0 & v_2(0) \end{bmatrix}\begin{bmatrix} 1-\theta_2 & \theta_1 \\ \theta_2 & 1-\theta_1 \end{bmatrix} \tag{50}$$

which coincides with the expression given by Qureshi and Wei[21]. The transient concentration profiles are obtained by solving the continuity relations

$$\frac{\partial(\theta)}{\partial t} = \nabla\cdot[[D^s]\nabla(\theta)] \tag{51}$$

An alternative formulation is to define effective surface diffusivities $D_{i,\text{eff}}^s$:

$$\frac{\partial\theta_i}{\partial t} = \nabla\cdot(D_{i,\text{eff}}^s\nabla\theta_i) \quad i = 1, 2 \tag{52}$$

By comparing Equation (52) with Equations (49) and (51), we obtain the following expressions for the effective diffusivities of components 1 and 2:

$$D_{1,\text{eff}}^s = \frac{Đ_1^s}{(1-\theta_1-\theta_2)}\left((1-\theta_2)+\theta_1\frac{\nabla\theta_2}{\nabla\theta_1}\right)$$

$$D_{2,\text{eff}}^s = \frac{Đ_2^s}{(1-\theta_1-\theta_2)}\left((1-\theta_1)+\theta_2\frac{\nabla\theta_1}{\nabla\theta_2}\right) \tag{53}$$

The above Expressions (53) for the effective surface diffusivities in a binary mixture coincide precisely with those given by Round *et al*[22]. It is clear from Equations (53) that the effective surface diffusivities are strong functions of surface concentrations and surface concentration gradients. Farooq and Ruthven[1] have used these Equations (53) to simulate the kinetically controlled PSA process for separation of a mixture of oxygen and nitrogen.

In order to demonstrate some of the key features of surface diffusion, Van den Broeke *et al.*[23] solved Equations (50) and (51) for single-file transient uptake of components 1 and 2 inside a plane sheet. Their solution for the transient profiles of surface occupancies, using the analytic procedure developed by Krishna[12], is shown in *Figure 9a*. The maximum in the surface occupancy of the faster moving component 2 is noteworthy. This

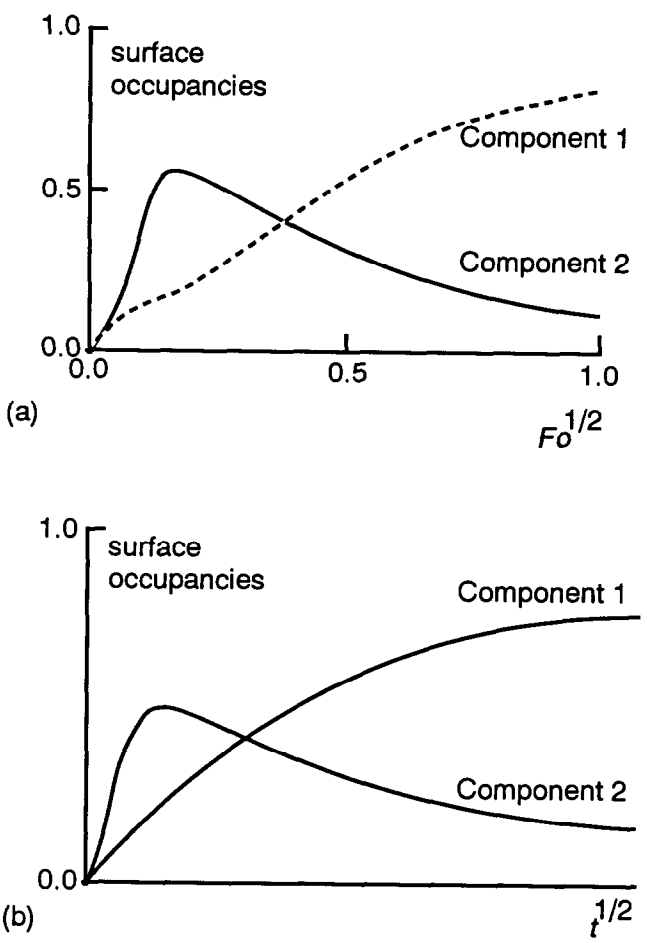

Figure 9 Transient uptake of components 1 and 2 inside a spherical microporous particle. The y-axis shows the surface occupancies of components 1 (θ_1) and 2 (θ_2). (a) Transient profiles obtained by solution of Equations (50) and (51) taking $v_2(0) = 50v_1(0)$. The saturation concentrations are assumed to be $\theta_1(t \to \infty) = 0.85$; $\theta_2(t \to \infty) = 0.10$. The Fourier number Fo is defined as $Fo \equiv Đ_1^s t/r_c^2$. (b) Monte Carlo simulations for a square lattice for the same set of conditions as in (a) above. The results are due to Van den Broeke *et al*[23].

maximum concentration is significantly higher than the ultimate equilibrium value $\theta_2(t \to \infty) = 0.10$. Van den Broeke *et al.*[23] also performed Monte Carlo simulations with the single-file diffusion model to obtain the results shown in *Figure 9b*. These results are in agreement with the predictions of the Maxwell–Stefan surface diffusion equations in *Figure 9a*.

The curious maximum for component 2 observed in *Figure 9* can be explained physically as follows. The surface mobility, reflected in the Maxwell–Stefan surface diffusivity, of component 2, $Đ_2^s$, is fifty times larger than the corresponding mobility of component 1, $Đ_1^s$. Initially, therefore, component 2 quickly penetrates the pores of the microporous solid. The adsorption strength of component 2 ($\theta_2(t \to \infty) = 0.10$) is considerably lower than that of component 1 ($\theta_1(t \to \infty) = 0.85$). Beyond the time corresponding to the maximum in component 2 concentration, the relatively poorly adsorbed component 2 gets (slowly) displaced from the active sites by component 1 and the surface concentration of component 2 decreases from its maximum value to reach, eventually, its final low equilibrium concentration.

The qualitative features of the transient behaviour sketched in *Figure 9* has been experimentally confirmed by Kärger and Bülow[24] for uptake of benzene and *n*-heptane in NaX zeolite. Two kinds of process can be devised for separating benzene (1) and *n*-heptane (2). An equilibrium separation process, requiring about 5 h of contact, will result in the pores of the zeolite filled predominantly with the strongly adsorbed benzene. Krishna[13] has pointed out the specific advantages of restricting the contact time to correspond to the maximum in the component 2 profile. This results in diffusion selectivity towards the poorly adsorbed *n*-heptane. A diffusive selective process could result in much smaller equipment sizes.

For single-file diffusion of an *n*-component mixture, the Fickian surface diffusivity matrix is given by Equation (43). If it is further assumed that the surface diffusivities $Đ_i^s$ are given by Equations (31), the following expression for the Fickian surface diffusivity matrix is obtained:

$$[D^s] = \lambda^2 \begin{bmatrix} v_1(0) & 0 & 0 & 0 \\ 0 & v_2(0) & 0 & 0 \\ 0 & 0 & \ddots & 0 \\ 0 & 0 & 0 & v_n(0) \end{bmatrix} [\Gamma] \qquad (54)$$

Van den Broeke *et al.*[23] solved Equations (51) and (54) for a ternary mixture for which the frequencies $v_i(0)$ were in the ratio 1:10:50. The transient uptake profiles are shown in *Figure 10a* for the Maxwell–Stefan model. Both components 2 and 3 exhibit maxima, suggesting a diffusion selective process for separating this ternary mixture. The Monte Carlo simulation results for the same set of conditions (*Figure 10b*) show qualitative agreement with the Maxwell–Stefan model predictions.

Surface diffusion with adsorbate–adsorbate interactions

In the general case of adsorbate–adsorbate interactions the Fickian surface diffusivity matrix has to be evaluated by using Equations (40)–(42). These calculations will be illustrated by considering a two-component system.

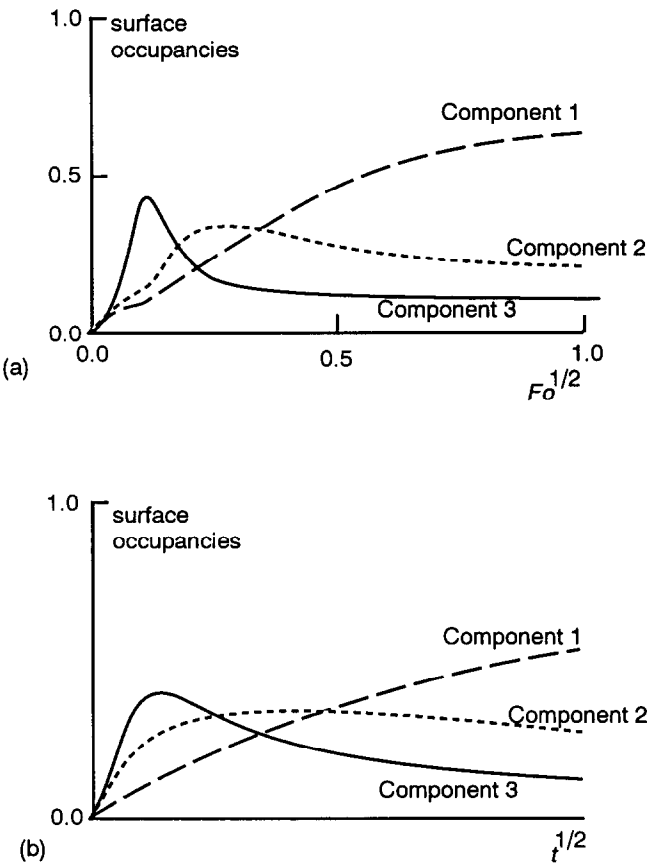

Figure 10 Transient uptake of components 1, 2 and 3 inside a spherical microporous particle. The *y*-axis shows the surface occupancies of components 1(θ_1), 2(θ_2) and 3(θ_3). (a) Transient profiles obtained by solution of Equations (50) and (54) taking $v_3(0) = 5v_2(0) = 50v_1(0)$. The saturation concentrations are assumed to be $\theta_1(t \to \infty) = 0.65$; $\theta_2(t \to \infty) = 0.20$; $\theta_3(t \to \infty) = 0.10$. The Fourier number Fo is defined as $Fo \equiv Đ_1^s t/r_c^2$. (b) Monte Carlo simulations for a square lattice for the same set of conditions as in (a) above. The results are due to Van den Broeke *et al.*[23]

Assuming the Langmuir isotherm, the Fickian surface diffusivity matrix reduces in this case to

$$[D^s] = \begin{bmatrix} \dfrac{1}{Đ_1^s} + \dfrac{\theta_2}{Đ_{12}^s} & -\dfrac{\theta_1}{Đ_{12}^s} \\ -\dfrac{\theta_2}{Đ_{12}^s} & \dfrac{1}{Đ_2^s} + \dfrac{\theta_1}{Đ_{12}^s} \end{bmatrix}^{-1} \times \frac{\begin{bmatrix} (1-\theta_2) & \theta_1 \\ \theta_2 & (1-\theta_1) \end{bmatrix}}{(1-\theta_1-\theta_2)} \qquad (55)$$

Calculations of the four elements of the Fickian surface diffusivity matrix using Equation (55) have been made in *Figure 11* for two cases: (i) $\theta_1 = 0.3$, $\theta_2 = 0.1$, and (ii) $\theta_1 = 0.2$, $\theta_2 = 0.2$. These calculations were made assuming that the counter-sorption diffusivity $Đ_{12}^s = Đ_2^s$, the *lower* of the two Maxwell–Stefan surface diffusivity values. The Maxwell–Stefan surface diffusion model calculations can now be compared with the Monte Carlo simulation results of Palekar and Rajadhyaksha[25] for diffusion in a zeolitic structure made up of parallel, non-intersecting channels. As can be seen from the results in *Figure 11*, the predictions of the Maxwell–Stefan equations agree remarkably well with the Monte Carlo results. The benefit of using the Maxwell–Stefan approach should be obvious because the elements of the matrix $[D^s]$ can be predicted from information on the values of $Đ_i^s$ and the adsorption isotherm.

To illustrate the differences between the calculations using Equation (55) (model including adsorbate–adsorbate exchange) and Equation (49) (single-file diffusion model without adsorbate–adsorbate exchange) calculations using both Equations (55) and (49) were performed to estimate the cross-coefficient D_{21}^s of the matrix $[D^s]$. These calculations are presented in *Figure 12* in terms of a surface plot with the surface occupancies θ_1 and θ_2 as parameters. The differences in the two model predictions do not appear to be significant. The results of *Figure 12* show remarkable similarities to the Monte Carlo simulations of Dahlke and Emig[26]. Further attention needs to be paid to the determination of the proper way to model intraparticle diffusion in microporous materials such as zeolites. We need to obtain an unequivocal answer to the question whether to include adsorbate–adsorbate interactions or not.

Comparison of the Maxwell–Stefan and Onsager formulations

An alternative approach to surface diffusion is to use the Onsager formulation of irreversible thermodynamics[27]. In this formulation the surface fluxes are written as linear functions of the chemical potential gradients. For n-component systems we write

$$(N^s) = -c^{sat}[L^s]\frac{1}{RT}(\nabla\mu) \tag{56}$$

From the Onsager reciprocal relations we conclude that the matrix $[L^s]$ is symmetric, i.e.

$$L_{ik}^s = L_{ki}^s \quad i,k = 1,2,\ldots n \tag{57}$$

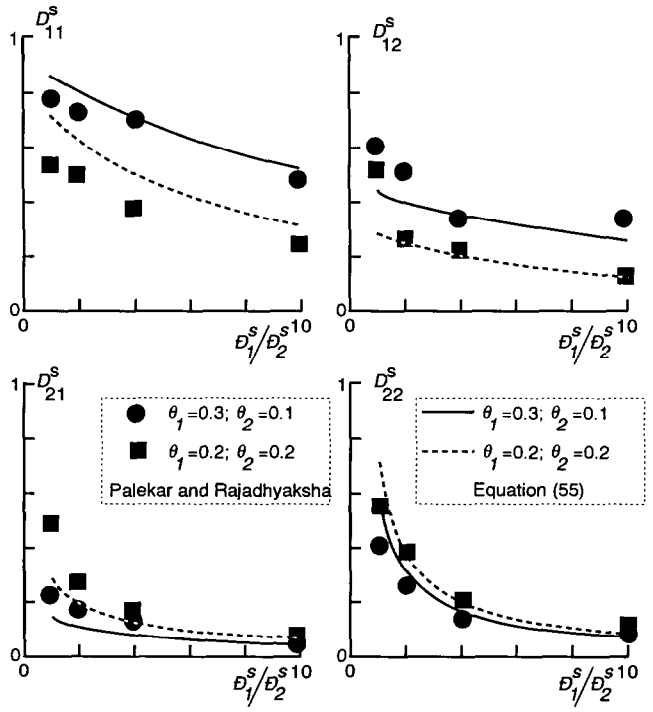

Figure 11 The elements of the Fickian surface diffusivity matrix, normalized with respect to D_{11}^s calculated at $\theta_1 = 0.4$; $\theta_2 = 0.0$, as a function of the ratio $Đ_1^s/Đ_2^s$. The curves refer to calculations using Equation (55). The points refer to the Monte Carlo simulation results of Palekar and Rajadhyaksha[25]

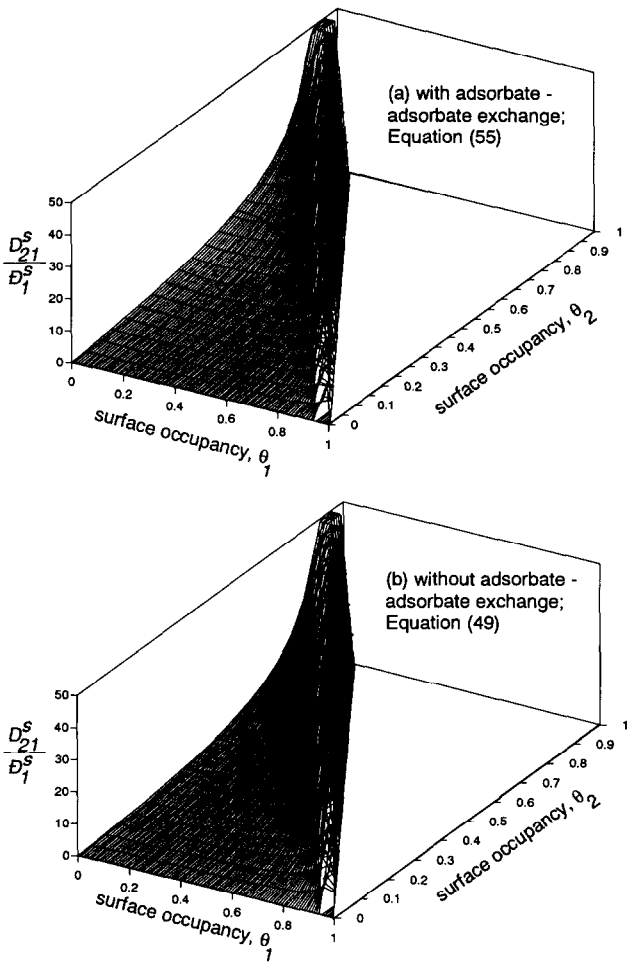

Figure 12 The cross-coefficient $D_{21}^s/Đ_1^s$ as a function of the surface occupancies θ_1 and θ_2. The following parameter values are used in the calculations: $Đ_2^s/Đ_1^s = 5$. (a) The calculations including the adsorbate–adsorbate counter-exchange (Equation (55)) with the exchange coefficient $Đ_{12}^s = Đ_1^s$. (b) The calculations using the single-file diffusion model without counter-exchange between the two adsorbates, Equation (49)

The chemical potential gradients may be related to the gradient of the surface occupancies (cf. Equation (34)):

$$\frac{1}{RT}\nabla\mu_i = \sum_{j=1}^{n}\frac{1}{p_i}\frac{\partial p_i}{\partial\theta_j}\nabla\theta_j = \frac{1}{\theta_i}\sum_{j=1}^{n}\Gamma_{ij}\nabla\theta_j \tag{58}$$

Combining Equations (56) and (58) gives:

$$(N^s) = -c^{sat}[L^s]\begin{bmatrix} 1/\theta_1 & 0 & 0 \\ 0 & \ddots & 0 \\ 0 & 0 & 1/\theta_n \end{bmatrix}[\Gamma](\nabla\theta) \tag{59}$$

Comparison of Equations (39) and (59) gives the relation between $[B^s]$ and $[L^s]$:

$$[B^s]^{-1} = [L^s]\begin{bmatrix} 1/\theta_1 & 0 & 0 \\ 0 & \ddots & 0 \\ 0 & 0 & 1/\theta_n \end{bmatrix}$$

$$[L^s]^{-1} = \begin{bmatrix} \theta_1 & 0 & 0 \\ 0 & \ddots & 0 \\ 0 & 0 & \theta_n \end{bmatrix}[B^s] \tag{60}$$

It can easily be verified by using matrix algebra that for the general case using Equations (40) for calculation of $[B^s]$, which includes adsorbate–adsorbate interactions, the Onsager reciprocal relations (57) are automatically satisfied. The Onsager formulation, though equivalent to the Maxwell–Stefan formulation, does not provide any direct method for predicting the off-diagonal elements of $[L^s]$. Yang *et al.*[27] had to resort to quite a complicated analysis to predict these off-diagonal elements. The use of Equation (32) for prediction of the counter-sorption diffusivity allows straightforward estimations of the matrix $[D^s]$. This procedure has been confirmed by comparison with Monte Carlo simulations (*Figure 11*). It can also be verified that the neglect of the off-diagonal elements in $[L^s]$ is tantamount to the use of the single-file diffusion model, Equation (43), i.e.

$$L_{ik(i\neq k)} = 0 \tag{61}$$

Combined bulk, Knudsen and surface diffusion

Setting up the Maxwell–Stefan diffusion equations for combined bulk, Knudsen and surface diffusion is a straightforward combination of the formalisms developed earlier in this paper. It is helpful to have a physical picture of the combined phenomena in mind. Towards this end the cratered dusty gas model is proposed. The large dust molecules, of infinite molar mass, representing the medium, have craters on their exterior surface representing the adsorption sites (*Figure 13*). Molecule–molecule collisions and molecule–dust collisions occurring in series result, respectively, in bulk and Knudsen diffusion. In addition, each of the molecular species may be adsorbed on the active sites of the medium. These vacant sites are also accorded the status of pseudo-species, of vanishing molar mass, and may be thought of as being akin to craters on a golf ball. The adsorbed species move ('hop' or 'jump') from one crater to another and may undergo desorption to the bulk fluid phase.

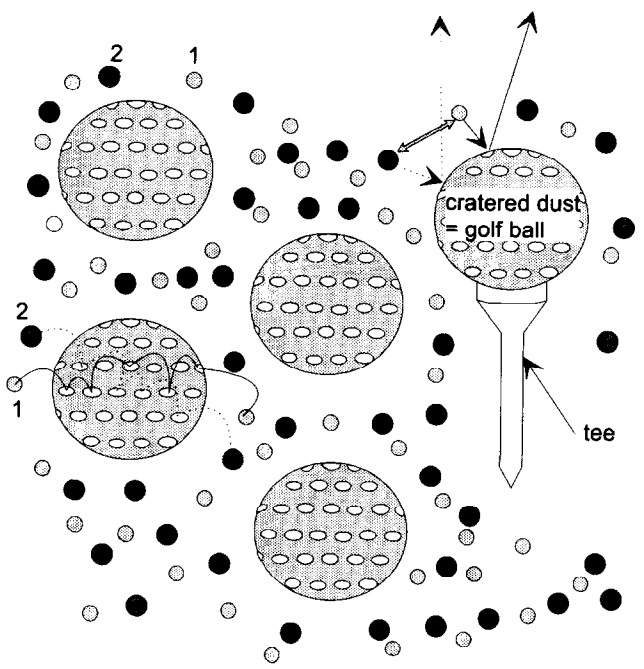

Figure 13 The three mechanisms of bulk, Knudsen and surface diffusion can be integrated into a common physical picture in which the porous medium is modelled as giant dust molecules (golf balls) with craters representing the adsorption sites

We may combine the (parallel) contributions of bulk and Knudsen (superscript b + K) and surface diffusion (superscript s) inside a porous adsorbent particle consisting of macropores (of porosity ϵ_{macro}) and micro-crystallites (see *Figure 1*)

$$N_i^{total} = \epsilon_{macro} N_i^{b+K} + (1-\epsilon_{macro}) N_i^s a_{micro} \tag{62}$$

where a_{micro} is the micropore surface area of the pore per unit per volume of the microcrystallites. The first term on the right-hand side of Equation (62), expressing the contributions of bulk and Knudsen diffusion, can be calculated by use of Equation (11). The second term on the right-hand side of Equation (62) is the contribution of the surface diffusion flux and is to be calculated from Equation (39).

Let us re-cast Equation (11) into the form

$$(N^{b+K}) = -\frac{1}{RT}[B^{b+K}]^{-1}(\nabla p) = -\frac{1}{RT}[D^{b+K}](\nabla p) \tag{63}$$

where the elements of the matrix $[B^{b+K}]$ are given by Equation (12). The surface flux N_i^s is similarly given by Equations (39)–(41):

$$(N^s) = -c^{sat}[D^s](\nabla\theta) = -c^{sat}[B^s]^{-1}[\Gamma](\nabla\theta) \tag{64}$$

An alternative form of Equation (64) is to use the gradients of loadings of the adsorbed species, expressed in terms of q_i (mol kg^{-1}):

$$(N^s) = -\frac{\rho_p}{a_{micro}}[D^s](\nabla q) = -\frac{\rho_p}{a_{micro}}[B^s]^{-1}[\Gamma](\nabla q) \tag{64a}$$

We may substitute Equations (63) and (64) in Equation (62) to obtain

$$(N^{total}) = -\frac{1}{RT}\epsilon_{macro}[B^{b+K}]^{-1}(\nabla p) - c^{sat}a_{micro}(1-\epsilon_{macro})[B^s]^{-1}[\Gamma](\nabla\theta) \tag{65}$$

It remains now to relate the gradients of the partial pressure in the bulk fluid phase (∇p) to the gradients of the surface occupancies ($\nabla\theta$). Note from Equation (34) that

$$\frac{\theta_i}{p_i}\nabla p_i = \sum_{j=1}^{n}\Gamma_{ij}\nabla\theta_j \tag{66}$$

If we define a diagonal matrix of distribution coefficients between the adsorbed species and the pore fluid:

$$K_i = \frac{a_{pore}c^{sat}RT\theta_i}{p_i} = \frac{\rho_p RTq_i}{p_i} \tag{67}$$

we obtain the following expression for the total flux

$$(N^{\text{total}}) = -\frac{1}{RT}\left[\epsilon_{\text{macro}}[B^{b+K}]^{-1} + (1-\epsilon_{\text{macro}})[B^{s}]^{-1} \times \begin{bmatrix} K_1 & 0 & 0 \\ 0 & \ddots & 0 \\ 0 & 0 & K_n \end{bmatrix}\right](\nabla p) \tag{68}$$

It is interesting to note that the thermodynamic factor $[\Gamma]$ has dropped out of the final working expression for the calculation of the fluxes. The separation of the drag effects (portrayed by the matrices $[B^{b+K}]$ and $[B^{s}]$) from the thermodynamic effects (portrayed by the matrix $[\Gamma]$) leads to significant simplifications in the computations, as is evidenced by the simple final form of the Equation (68). The intuitively simple expression (68) reinforces our faith in the Maxwell–Stefan formulation.

We may also express the total fluxes N_i^{total} in terms of the driving forces for surface diffusion, $\nabla\theta_i$, by introducing Equations (66) and (67) into Equation (68)

$$(N^{\text{total}}) = -a_{\text{micro}}c^{\text{sat}}\left[\epsilon_{\text{micro}}[B^{b+K}] + (1-\epsilon_{\text{macro}})[B^{s}]^{-1} \times \begin{bmatrix} K_1 & 0 & 0 \\ 0 & \ddots & 0 \\ 0 & 0 & K_n \end{bmatrix}\right] \times \begin{bmatrix} 1/K_1 & 0 & 0 \\ 0 & \ddots & 0 \\ 0 & 0 & 1/K_n \end{bmatrix}[\Gamma](\nabla\theta) \tag{69}$$

If the diffusion inside the macropores is governed by Knudsen diffusion then the matrix $[B^{b+K}]$ is given by Equation (21). Further, if adsorbate–adsorbate interactions in the matrix $[B^{s}]$ are neglected (cf. Equation (43)), the total fluxes across the adsorbent particle will be

$$(N^{\text{total}}) = -a_{\text{micro}}c^{\text{sat}}\left[\epsilon_{\text{macro}}\begin{bmatrix} \mathcal{D}_{1,Kn} & 0 & 0 \\ 0 & \ddots & 0 \\ 0 & 0 & \mathcal{D}_{n,Kn} \end{bmatrix} + (1-\epsilon_{\text{macro}})\begin{bmatrix} \mathcal{D}_1^{s} & 0 & 0 \\ 0 & \ddots & 0 \\ 0 & 0 & \mathcal{D}_n^{s} \end{bmatrix}\begin{bmatrix} K_1 & 0 & 0 \\ 0 & \ddots & 0 \\ 0 & 0 & K_n \end{bmatrix}\right] \times \begin{bmatrix} 1/K_1 & 0 & 0 \\ 0 & \ddots & 0 \\ 0 & 0 & 1/K_n \end{bmatrix}[\Gamma](\nabla\theta) \tag{70}$$

For the transient diffusion to a cylindrical adsorbent particle, the fractional uptake from a binary gas mixture at constant bulk composition is given by[12,29]

$$(\theta) = \left[[I] - 4\sum_{m=1}^{\infty}\frac{\exp\left(-\xi_m^2\frac{[D^{\text{total}}]}{D_{\text{ref}}}Fo\right)}{\xi_m^2}\right](\theta^{\text{sat}}) \tag{71}$$

where ξ_m represent the roots of the zero-order Bessel function $J_0(\xi_m) = 0$, D_{ref} is a reference value for the intraparticle diffusivity, and $Fo \equiv 4D_{\text{ref}}t/d_p^2$ is the Fourier number. The matrix $[D^{\text{total}}]$ represents the combined bulk, Knudsen and surface diffusion characteristics of the particle. Equation (71) may be evaluated by using matrix algebra[12]. To demonstrate the validity of this approach simulations are presented using Equation (71) for intra-particle diffusion of the binary gas mixtures ethane–*n*-butane, ethane–*n*-pentane and *n*-butane–*n*-pentane inside activated carbon[28]. In *Figure 14*

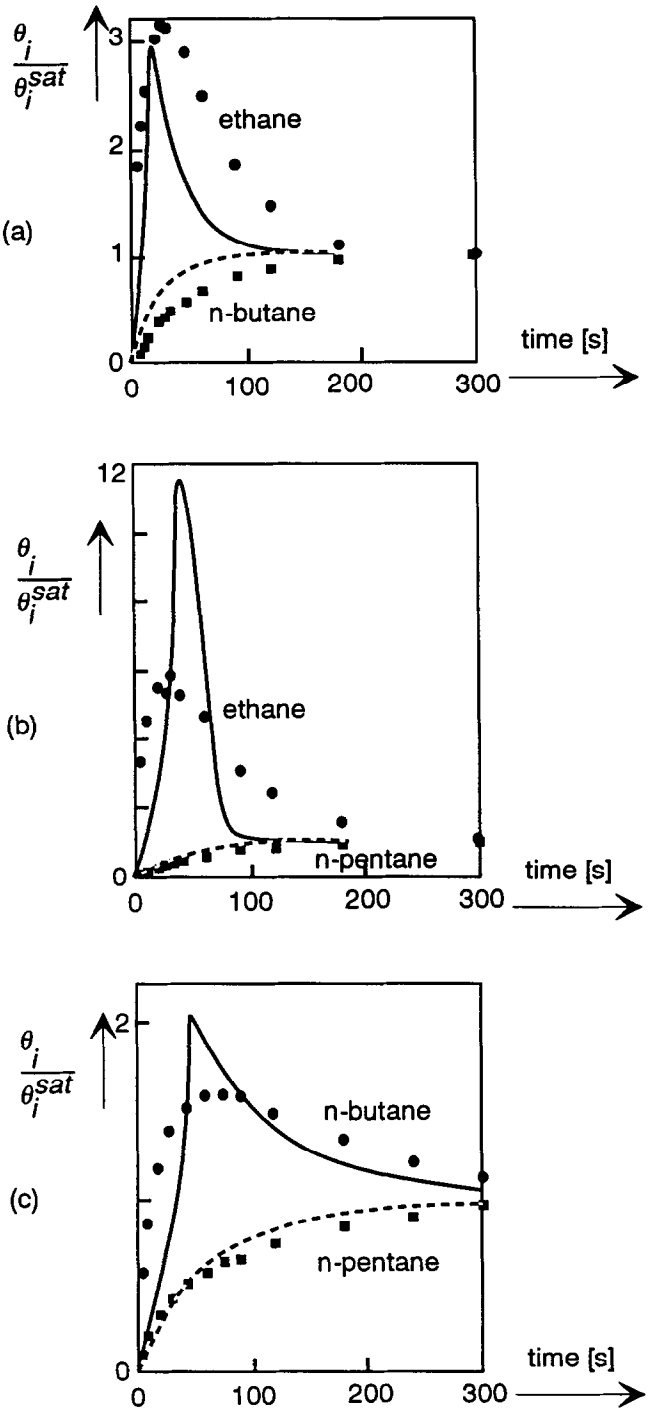

Figure 14 Uptake of binary gas mixtures in Ajax activated carbon: (a) uptake of ethane (1)–*n*-butane (2). (b) Uptake of ethane (1)–*n*-pentane (2). (c) Uptake of *n*-butane (1)–*n*-pentane (2). The experimental data are from Hu and Do[28]. The simulations are using the analytical solution (70) with the model parameters as given in *Table 1*

Table 1 Transient uptake of binary gas mixtures by activated carbon

	Figure 14a	*Figure 14b*	*Figure 14c*
Binary mixture	Ethane (1)–*n*-butane (2)	Ethane (1)–*n*-pentane (2)	*n*-butane (1)–*n*-pentane (2)
Bulk gas mixture Composition of components 1 and 2	28.6% 10.6%	28.5% 8.6%	21.8% 7%
Equilibrium *K*-values evaluated at bulk composition	$K_1 = 201$ $K_2 = 858$	$K_1 = 202$ $K_2 = 1066$	$K_1 = 457$ $K_2 = 1302$
Saturation occupancies of components 1 and 2	$\theta_1^{sat} = 0.179$ $\theta_2^{sat} = 0.801$	$\theta_1^{sat} = 0.032$ $\theta_2^{sat} = 0.948$	$\theta_1^{sat} = 0.271$ $\theta_2^{sat} = 0.709$
Knudsen diffusivity inside macropores (10^{-6} m^2 s^{-1})	$Đ_{1,Kn} = 1.852$ $Đ_{2,Kn} = 1.240$	$Đ_{1,Kn} = 1.852$ $Đ_{2,Kn} = 1.097$	$Đ_{1,Kn} = 1.240$ $Đ_{2,Kn} = 1.097$
Micro-pore (surface) diffusivities (10^{-9} m^2 s^{-1})	$Đ_1^s = 4.330$ $Đ_2^s = 0.932$	$Đ_1^s = 4.330$ $Đ_2^s = 0.315$	$Đ_1^s = 0.932$ $Đ_2^s = 0.315$

Pressure, $p = 101.35$ kPa; temperature, $T = 303.15$ K; macroporosity, $\epsilon_{macro} = 0.31$; particle diameter, $d_p = 1.588$ mm

the predictions of Equation (71) taking

$$[D^{total}] = \begin{bmatrix} \epsilon_{macro} \begin{bmatrix} Đ_{1,Kn} & 0 & 0 \\ 0 & \ddots & 0 \\ 0 & 0 & Đ_{n,Kn} \end{bmatrix} \\ +(1-\epsilon_{macro}) \begin{bmatrix} Đ_1^s & 0 & 0 \\ 0 & \ddots & 0 \\ 0 & 0 & Đ_n^s \end{bmatrix} \begin{bmatrix} K_1 & 0 & 0 \\ 0 & \ddots & 0 \\ 0 & 0 & K_n \end{bmatrix} \end{bmatrix} \times \begin{bmatrix} 1/K_1 & 0 & 0 \\ 0 & \ddots & 0 \\ 0 & 0 & 1/K_n \end{bmatrix} [\Gamma] \quad (72)$$

are compared with the experimental data of Hu and Do[28]. The model parameters used in Equations (71) and (72) are summarized in *Table 1*. These parameters were determined by Hu and Do[28]. The essential features of the transient uptake profiles are reproduced by the simple analytical model developed here. Further, the agreement between simulations and experiment is almost as good as that presented by Hu and Do[28], who used a numerical solution of the partial differential equations representing macro- and micro-pore diffusion. The simple approach outlined above is recommended for designing adsorption columns.

Conclusions

In this paper an attempt has been made to model intraparticle diffusion inside a porous medium in a unified consistent manner by using a simple mechanistic picture of diffusion. To move a species with respect to other species (i.e. to allow a species to diffuse) we must exert a force on it; this force is the gradient of the chemical potential. During species diffusion drag is encountered with other molecular species and we have a balance between the applied force and frictional drag with the other molecular species. By using this simple, hydrodynamic, model, i.e. the Maxwell–Stefan formulation, we set out to model, in turn, bulk, Knudsen and surface diffusion. The considerable advantages of the Maxwell–Stefan approach have been demonstrated by means of several examples.

References

1 **Farooq, S. and Ruthven, D.M.** *Chem Engng Sci* (1991) **46** 2213–2224
2 **Sircar, S.** *Proc 3rd Int Conf Fundam Adsorption* Sonthofen, Germany (1991) 815–843
3 **Ruthven, D.M.** *Principles of Adsorption and Adsorption Processes* John Wiley, New York (1984)
4 **Jackson, R.** *Transport in Porous Catalysts* Elsevier, Amsterdam (1977)
5 **Mason, E.A. and Malinauskas, A.P.** *Gas Transport in Porous Media: The Dusty Gas Model* Elsevier, Amsterdam (1983)
6 **Maxwell, J.C.** *Phil Trans Roy Soc Lond* (1987) **157** 49
7 **Stefan, J.** *Sitzber Akad Wiss Wien* (1871) **63** 63
8 **Reid, R.C., Prausnitz, J.M. and Poling, B.E.** *The Properties of Gases and Liquids* 4th Edn, McGraw-Hill, New York (1988)
9 **Duncan, J.B. and Toor, H.L.** *AIChE J* (1962) **8** 38–41
10 **Toor, H.L.** *AIChE J* (1957) **3** 198–207
11 **Gilliland, E.R., Baddour, R.F., Perkinson, G.P. and Sladek, K.J.** *Ind Eng Chem Fundam* (1974) **13** 95–100
12 **Krishna, R.** *Chem Engng Sci* (1990) **45** 1779–1791
13 **Krishna, R.** *Chem Engng Sci* (1993) **48** 845–861
14 **Reed, D.A. and Ehrlich, G.** *Surface Sci* (1981) **102** 588–609; *ibid* **105** 603–628
15 **Riekert, L.** *AIChE J* (1971) **17** 446–454
16 **Zhdanov, V.P.** *Surface Sci* (1985) **194** L13–L17
17 **Barrer, R.M.** *Zeolites and Clay minerals as Sorbents and Molecular sieves* Academic Press, London (1978)
18 **Yang, R.T.** *Gas Separation by Adsorption Processes* Butterworth, Boston (1987)
19 **Ruthven, D.M., Xu, Z. and Farooq, S.** Sorption kinetics in PSA systems *Gas Sep Purif* (1993) **7** 75–81 (this issue)
20 **Garg, D.R. and Ruthven, D.M.** *Chem Engng Sci* (1972) **27,** 417–423
21 **Qureshi, W.R. and Wei, J.** *J Catal* (1990) **126,** 126–146
22 **Round, G.F., Habgood, H.W. and Newton, R.** *Sep Sci* (1966) **1** 219–244.
23 **Broeke, L.J.P. van den, Nijhuis, S. and Krishna, R.** *J Catal* (1992) **136** 463–477
24 **Kärger, J. and Bülow, M.** *Chem Engng Sci* (1975) **30** 893–896
25 **Palekar, M.G. and Rajadhyaksha, R.A.** *Chem Engng Sci* (1986) **41** 463–468
26 **Dahlke, K. and Emig, G.** *Catalysis Today* (1991) **8** 439–450
27 **Yang, R.T., Chen, Y.D. and Yeh, Y.T.** *Chem Engng Sci* (1991) **46** 3089–3099
28 **Hu, X. and Do, D.D.** *Chem Engng Sci* (1992) **47** 1715–1725
29 **Crank, J.** *The Mathematics of Diffusion* Oxford University Press (1975)